***Manuscript accepted for publication in* Chemical Physics**

Substituent position effects on sunscreen photodynamics: a closer look at methyl anthranilate

Natércia d. N. Rodrigues[1], Neil C. Cole-Filipiak[1], Matt A. P. Turner,[1,2] Konstantina Krokidi[1], Georgia L. Thornton[1], Gareth W. Richings[1], Nicholas D. M. Hine[2], and Vasilios G. Stavros[1*]

[1]*University of Warwick, Department of Chemistry, Coventry, CV4 7AL, UK*

[2]*University of Warwick, Department of Physics, Coventry, CV4 7AL, UK*

**Corresponding author's e-mail: V.Stavros@warwick.ac.uk*

Towards the development of a *bottom-up* rationale for sunscreen design, the effects of substituent position on the ultrafast photodynamics of the sunscreen precursor methyl anthranilate (MA, an *ortho* compound) were evaluated by studying *para*- and *meta*-MA in vacuum. Time-resolved ion yield (TR-IY) measurements reveal a long-lived S_1 excited state ($\gg$ 1.2 ns) for *para*-MA, proposed to be the result of a weakly fluorescent, bound excited state. In the case of *meta*-MA, TR-IY transients reveal a much faster (~2 ns) excited state relaxation, possibly due to multiple low-lying S_1/S_0 conical intersections of prefulvenic character. While *meta*-MA may not be an ideal sunscreen ingredient due to a low ultraviolet absorbance, its comparatively efficient relaxation mechanism may constitute an alternative to common sunscreen relaxation pathways. Thus, our results should prompt further studies of prefulvenic relaxation pathways in potential sunscreen agents.

Keywords: photoprotection; sunscreen; photochemistry; CASPT2; conical intersection; excited state

Introduction

The harmful effects of ultraviolet (UV) radiation on living organisms have been extensively reported in the literature.[1–5] UVB radiation (315–280 nm) can be directly absorbed by DNA in human skin, leading to photolesions which may potentially lead to skin cancer.[2,5,6] Even though skin has its own natural means of photoprotection in the form of melanin pigments,[7] this is often insufficient and erythema (sunburn) may still occur.[6] Sunscreen lotions, which consist of a complex mixture of UV absorbing species and other ingredients, can be used for extra photoprotection. Nevertheless, and despite the wide availability of sunscreen products on the market, skin cancer incidence has risen in recent years.[8] The urgency for better sunscreens which are designed for optimum photoprotection is, therefore, evident.

An ideal sunscreen molecule should be able to safely and efficiently dissipate the excess energy resulting from absorption of UV radiation so as to avoid potentially harmful side reactions such as fragmentation of the sunscreen molecule and subsequent free radical release or reaction with (or energy transfer to) other components in the sunscreen lotion or the skin itself.[9–11] Fast energy dissipation mechanisms – on an ultrafast timescale (femto to picoseconds, 10^{-15} to 10^{-12} s, respectively) – accessible to the sunscreen molecule's excited state population facilitate relaxation from a given excited electronic state (S_n) to the ground electronic state (S_0) and thus avoid the aforementioned harmful side reactions.[9–11] Such energy dissipation mechanisms may involve a number of photophysical and/or photochemical pathways, usually jointly referred to as a molecule's photodynamics.

In employing a *bottom-up* development of novel sunscreen materials, by which their structure-dynamics-function relationships are studied for incremental molecular and environment complexity,[11] we have previously reported[12] on the photodynamics of the sunscreen precursor methyl anthranilate (*o*-MA, an *ortho* compound as shown in Figure

1). In an attempt to unveil the intrinsic photodynamics of *o*-MA, *i.e.* with no perturbations from the environment, we studied this molecule in vacuum and found that, upon photoexcitation within the UVA (400–315 nm) and UVB wavelength range, the first electronic excited state of *o*-MA (S_1) is accessed, and then observed to persist well beyond the temporal window of those experiments (1.2 ns). This long-lived behaviour, observed both in vacuum *and* in solution, is due to an intramolecular hydrogen bond between the amino and ester substituents.[12] The hydrogen bond traps excited state population on the S_1 surface of *o*-MA, hindering access to a nearby conical intersection (CI) along the ester internal rotation. To explore how the fundamental (*i.e.* without environment perturbations) photodynamics of *o*-MA are altered by the absence of the intramolecular hydrogen bond, we have investigated the gas-phase (in vacuum) excited state dynamics of both *para*- and *meta*-MA (herein referred to as *p*-MA and *m*-MA, respectively; see Figure 1 for structures).

Systems structurally similar to *p*-MA have received considerable attention in the literature (see reference 13 and references therein). In a sunscreen context, the carboxylic acid analogue of *p*-MA, *para*-aminobenzoic acid or PABA, was widely used in the 1930s and 1940s in sunscreen formulations, but is now avoided due to its allergic and photoallergic potential.[14] *Para*-aminobenzoates, and other such systems for which electron donating and withdrawing substituents are positioned *para* to each other, have a twisted intramolecular charge transfer (TICT) state accessible upon photoexcitation, though such states are not observed in vacuum.[15,16] Previous two-colour resonant two-photon ionisation (R2PI) studies on *p*-MA yielded sharp spectra, suggesting long-lived excited states for this molecule.[17] Indeed, *p*-MA and similar molecules are known to fluoresce in vacuum[16,18–20] though, to the best of our knowledge, the complete relaxation mechanisms of *p*-MA have not been investigated. In comparison with *p*-MA, *m*-MA is relatively understudied in the literature.

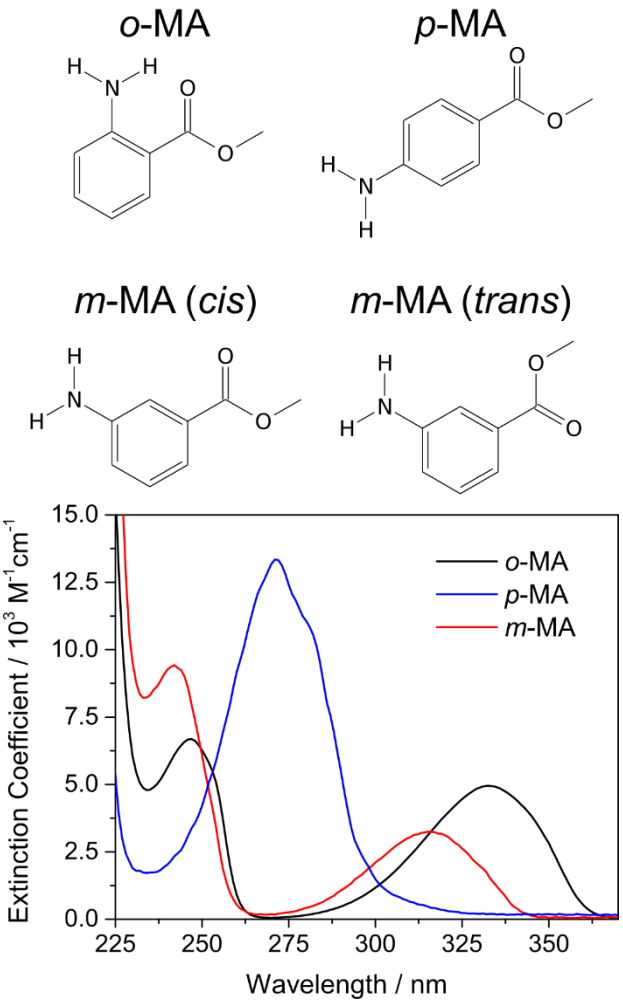

Figure 1: Ultraviolet absorption spectra of *o*-MA (green), *m*-MA (red) and *p*-MA (blue) in cyclohexane. The *o*-MA spectrum has been reproduced from reference 12. The molecular structures of each molecule are also shown, including the rotamers of m-MA.

Nevertheless, in the gas-phase, two rotamers around the C_{ring}–$C_{carbonyl}$ bond (see Figure 1) have been identified by laser induced fluorescence;[20,21] both rotamers have nearly identical S_1 origin transition energies.

In the present work, we provide time-resolved information on the fundamental relaxation mechanisms undergone by photoexcited *p*-MA and *m*-MA in vacuum; we shall then compare our observations to our previously reported observations for *o*-MA, thus exploring the intrinsic effects of substituent position on the photodynamics of the anthranilates. We suggest a relaxation pathway for *m*-MA which may serve as an alternative to the mechanisms commonly observed in current sunscreen

molecules.[11] This fundamental work has the potential to allow for targeted development and selection of sunscreen molecule candidates by matching desirable photophysical behaviours with trends in molecular structure. Such a comprehensive understanding of sunscreen photophysics will inform the *bottom-up* design of the next generation of photoprotective materials.[10,11]

Experimental Methods

i. Absorption and Fluorescence Spectra

Absorption spectra in the ultraviolet and visible (UV/Vis) wavelength ranges were obtained for methyl 4-aminobenzoate (*p*-MA; Sigma Aldrich, 98%) and methyl 3-aminobenzoate (*m*-MA; Alfa Aesar, > 98%) using a Cary 60 UV/Vis spectrometer. These measurements were performed on solutions of *p*-MA and *m*-MA solvated in cyclohexane at a concentration of approximately 10^{-6} M.

The fluorescence spectra of *p*-MA and *m*-MA in room temperature (~22°C), air saturated cyclohexane were recorded with photoexcitation at 289.6 and 320.2 nm, respectively, using a Horiba Scientific Fluorolog 3. The fluorescence quantum yield at these wavelengths was measured by comparing to solutions of *trans,trans*-1,4-diphenyl-1,3-butadiene in room temperature, air saturated cyclohexane.[22] The fluorescence lifetime of *m*-MA in cyclohexane was recorded using a 320 nm NanoLED (Horiba Scientific) attached to the Fluorolog. The resulting time-resolved fluorescence signal was fit with the Horiba DAS6 Analysis software package using a single exponential decay convoluted with the instrument response function. Further details of the fluorescence study may be found in section C of the Supplementary Material (SM).

ii. Time-Resolved Ion Yield (TR-IY)

The experimental setup has been thoroughly described before[23–25] and therefore only a brief overview is provided here. A fundamental laser beam, with a central wavelength of 800 nm, *ca.* 40 fs temporal full width at half maximum (FWHM) and 3 mJ per pulse, was generated from a commercial femtosecond Ti:sapphire oscillator (Spectra-Physics Tsunami) and a regenerative amplifier (Spectra-Physics Spitfire XP). This beam was split into three equal parts of ~ 1 mJ per pulse, two of which were used to pump two optical parametric amplifiers (Light Conversion, TOPAS-C), producing the pump and the probe pulses. The samples were vaporised by heating to their respective melting points (approximately 135°C for *p*-MA and 140°C for *m*-MA), and subsequently seeded into helium gas (3 bar); the gaseous mixture was then expanded into a vacuum (~10^{-7} mbar) *via* an Even-Lavie pulsed solenoid valve,[26] thus forming a molecular beam.

The pump and probe beams intersected the molecular beam perpendicularly at the interaction region and were temporally delayed with respect to each other (at predefined pump-probe time delays Δt) by using a retroreflector mounted on a motorised delay stage in the pump beam path, yielding a maximum Δt of 1.2 ns. The pump wavelength, λ_{pu}, was selected in order to photoexcite the first electronic excited state of each molecule. Due to the proximity of the S_1 and S_2 states of *p*-MA,[27] we have photoexcited the molecule at λ_{pu} = 292 nm to ensure preferential population of the S_1 state near the S_1 origin.[20,27] In the case of *m*-MA, the pump wavelength was centred at both λ_{pu} = 325 nm (the S_1 origin[21]) and, to evaluate the effects of photoexciting the S_1 state of *m*-MA with higher energy, λ_{pu} = 300 nm. The probe wavelength, λ_{pr}, was then selected to allow for photoionisation of the photoexcited species and to minimise probe-initiated photodynamics: λ_{pr} = 315 nm for *p*-MA and 273 nm for *m*-MA. All UV laser pulses are broad in energy with approximately 0.06 eV FWHM; values of λ_{pu} and λ_{pr} are the central wavelength within this range.

The pump-probe ion signal was monitored by a detector consisting of two microchannel plates (MCPs) coupled to a metal anode. The current output from the anode, gated in ion flight time over the mass channel of each parent ion (*m*-MA^+ and *p*-MA^+), was measured on a digital oscilloscope (LeCroy LT372

Waverunner) and integrated as a function of Δt in order to produce time-resolved ion yield (TR-IY) transients. The magic angle equivalent transients were calculated from separate measurements for which the polarisation of the pump and probe beams were held either parallel or perpendicular relative to each other.[28] The quoted excited state lifetimes are extracted from modelling these transients by a sum of exponential decays convoluted with a Gaussian instrument response function; reported errors are the standard error from the fit. Additional details regarding kinetic fits may be found in section B of the SM.

Power dependence studies were performed to ensure linear signal *vs.* laser power, *i.e.* that no multiphoton events altered the observed dynamics. As described in section D of the SM, H^+ velocity map ion imaging experiments were also performed to investigate N–H bond dissociation.

Computational Methods

i. Density Functional Theory

Initial scans along portions of the electronic potential energy surfaces were conducted using density functional theory (DFT) using NWChem.[29] The structures of *p*-MA and *m*-MA were generated using Visual Molecular Dynamics molefacture plugin;[30] these structures were then optimised to obtain the corresponding ground electronic state molecular geometries with DFT at the PBE0[31]/cc-pVTZ[32] level of theory. In both species, several reaction coordinates were explored including the ester internal rotation, amine internal rotation, and N–H bond fission. Further details of all DFT methods may be found in section E of the SM.

ii. CASSCF/CASPT2

Relaxed geometries for *p*-MA and both rotamers of *m*-MA (see Figure 1) were taken from the DFT results described above. Singlet vertical excitation energies were calculated at each of these geometries using complete active space self-consistent field (CASSCF) calculations[33,34] with second-order perturbation theory (CASPT2) corrections[35–37] and the 6-311G* basis set[38,39] in Gaussian 03.[40] The active space used for these calculations comprised ten electrons and ten orbitals (10/10). The filled orbitals comprised two n orbitals and three π orbitals, with three π* orbitals and two Rydberg orbitals composing the valence space; see section F of the SM for diagrams of all orbitals.

A number of conical intersection searches were conducted using state averaged CASSCF[33,34] (SA-CASSCF) starting from each of the initial geometries to find potential conical intersections (CIs) between the S_0 and S_1 states. After observing the presence of prefulvenic ring distortions involved in the initial CI results (see below), a number of other prefulvenic structures were used as starting geometries in order to investigate the possibility of further conical intersections. These SA-CASSCF calculations used a reduced active space (6/6) and basis set (6-31G*),[39] again using Gaussian 03.[40] As an illustrative evaluation of the excited state potential energy surfaces, a linear interpolation of internal coordinates (LIIC) was used to generate steps between the vertical Franck-Condon region and CI geometries. Each of these steps were evaluated using SA-CASSCF(6,6) to get the relative S_0 and S_1 energies.

Results and Discussion

We start our discussion by noting the differences in ultraviolet absorption between the different MA derivatives, as shown in Figure 1. The *meta* isomer appears to retain the broad absorption peak previously observed for *o*-MA in the ~290–370 nm region,[12] despite a blue shift and decrease in extinction coefficient. The absorption spectrum is drastically changed, however, for *p*-MA: a prominent absorption feature is centred around 270 nm with a slight shoulder near 280 nm, previously assigned to the S_1 state.[27]

Since our broadband pump pulses will excite both *m*-MA rotamers and – as shown in section E of the SM – the electronic excited states of

the two *m*-MA rotamers appear to be nearly identical, results will be interpreted as coming from both rotamers. Table 1 shows the singlet excited state energies for *p*-MA and *m*-MA evaluated at the CASPT2(10,10) level of theory. The calculations for *m*-MA predict the $S_1 \leftarrow S_0$ transition at 3.79 eV which is remarkably close to the experimental value (~3.81 eV).[21] Unfortunately, the S_1 energy for *p*-MA is in poor agreement with the literature values.[17,20,27] This disagreement may be due to the significant ππ* character in our CASPT2 calculations, in disagreement with the pure nπ* character previously assigned to the $S_1 \leftarrow S_0$ transition.[41] Interestingly, our calculated S_1 origin is still within the long wavelength tail in the vapour phase absorption spectrum of *p*-MA.[27]

Table 1: Excited state properties for *p*-MA and *m*-MA at the CASPT2(10,10) level of theory. Fractional transition compositions are given in parenthesis.

Species (state)	Character	Energy (eV)
p-MA (S_1)	π* ← π (0.60) π* ← n (0.25)	3.65
p-MA (S_2)	π* ← π	4.66
m-MA (S_1)	π* ← π	3.79
m-MA (S_2)	π* ← π	4.17

We have previously reported the S_1 state of *o*-MA to be long-lived (> 1.2 ns) due to stabilisation of the excited state by an intramolecular hydrogen bond.[12] Regardless of the absence of an intramolecular hydrogen bond in *p*-MA, an equally long-lived excited state is observed upon photoexcitation to its S_1 state (as shown in Figure 2), in agreement with the predictions from previous frequency-resolved measurements.[17] The dominant, long-lived component of the *p*-MA TR-IY transient suggests that the excited state population is trapped, limited to intersystem crossing (ISC) and/or radiative decay. ISC may be facilitated by efficient coupling between the ^{1}nπ* state and a ^{3}ππ* state,[42] such as the T_1 state in *p*-MA,[43] eventually resulting in phosphorescence. Simultaneously, the at least partial nπ* character of the S_1 state (see Table 1) will hinder fluorescent decay due to the weak π* → n transition strength. We note the presence of a small intensity, ultrafast decay (~70 fs) in the TR-IY transients obtained for *p*-MA. As λ_{pu} = 292 nm should primarily excite the S_1 origin of *p*-MA,[17,20,27] it is unlikely that the observed decay is due to intramolecular vibrational energy redistribution. Moreover, our power dependency studies have shown that the ~70 fs component remains present upon lowering of the pump laser power. In addition, examination of the separate parallel and perpendicular polarisation transients (from which the presented magic angle equivalent

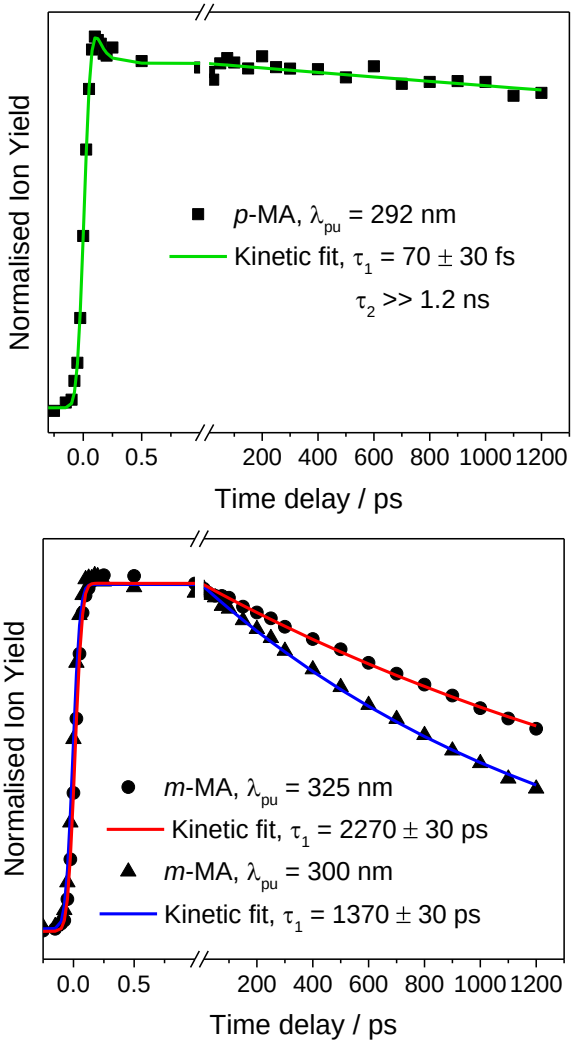

Figure 2: TR-IY transients for *p*-MA photoexcited at 292 nm (top) and *m*-MA photoexcited at 325 nm and 300 nm (bottom). Data are shown as black squares, circles and triangles, respectively, while the coloured lines correspond to kinetic fits, details of which are given in the SM. The time constants extracted from kinetic fits are also shown.

transients were produced) suggests that the observed ultrafast component could be a result of the magic angle equivalent transient failing to negate rotational effects, likely due to experimental conditions changing slightly between the parallel and perpendicular transients. While the exact nature of this short lifetime is unclear, the existence of an apparently minor ultrafast process does not alter our overall conclusions regarding the long-lived electronic excited state.

While the most significant differences observed in the absorption spectra are between either *o*-MA or *m*-MA and *p*-MA, the TR-IY transients of *m*-MA are the most distinct from the other two compounds. The *m*-MA transients, also shown in Figure 2, reveal significantly shorter S_1 state lifetimes (approximately 2 ns) when compared to *o*-MA or *p*-MA. Furthermore, there is a noticeable decrease in *m*-MA lifetime with decreasing wavelength. We note that, while 2 ns is outside of our temporal window and thus the values may not be accurate, we nonetheless quote the lifetime returned by our kinetic fit to guide discussion. In accordance with the original postulate of Domcke and co-workers,[44] the significant *m*-MA excited state decay observed could be mediated by dissociative πσ* states localised along the N–H stretch coordinate. Such ultrafast photoprotection mechanisms, important in biological systems, may be investigated in the gas-phase by looking for production of neutral H-atoms following photoexcitation; see reference 45 and references therein for examples. However, as shown in section D of the SM, resonantly probing H-atoms upon photoexcitation of *m*-MA revealed no evidence of H^+ signal that could be attributed to N–H bond dissociation *via* a πσ* state, though we note that H-atom loss may occur at longer time delays. Excited state calculations, shown in section E of the SM, confirm that near-origin population in the *m*-MA S_1 state is unlikely to access this dissociative coordinate. Hence, we conclude that a πσ* mediated decay mechanism does not play a significant role in the dynamics of the *m*-MA S_1 state.

It is plausible that the ~2 ns lifetime we extract from the *m*-MA TR-IY transients is due to highly efficient fluorescence in the gas-phase. While *m*-MA does fluoresce in vacuum,[20,21] neither the fluorescence lifetime nor a fluorescence quantum yield have been reported. Previous work[46,47] in our lab has shown that gas-phase dynamics may be qualitatively compared to measurements in cyclohexane, a minimally perturbing solvent. As such, we have measured the fluorescence lifetime of *m*-MA in cyclohexane, presented in Figure 3, to be 1.7 ns for *m*-MA and in excellent agreement with the excited state lifetime extracted from our gas-phase measurements. Furthermore, as shown in section C of the SM, we have also determined a fluorescence quantum yield of 25 ± 5% for *m*-MA in cyclohexane, substantially less than has been reported for *o*-MA.[48] These results suggest that while fluorescence is a dominant relaxation pathway for *m*-MA it is not solely responsible for the observed excited state decay lifetimes. While *m*-MA phosphorescence has been reported,[43] suggesting that ISC may be an important sink for S_1 state population, the total luminescence quantum yield of *m*-MA is less than unity and we must consider other non-radiative decay mechanisms.

In contrast with both *o*-MA and *m*-MA, the *p*-MA total luminescence quantum yield is less than 10% (see section C of the SM).[27,43] Additionally, the fluorescence lifetime of *p*-MA has been reported to be 0.89 ns,[27] in sharp contrast to the gas-phase lifetime observed in the present work. This strong disagreement is likely due to the $\pi^* \leftarrow n_{carbonyl}$ character of the S_1 state.[41] Such states are sensitive to local environment[49–51] and, as a result, the fluorescence results in solution are not comparable to our gas-phase TR-IY measurements.

In order to further explore the origins of the different gas-phase photodynamics observed for *p*-MA and *m*-MA, we have performed computational studies on both molecules, paying particular attention to any S_1/S_0 conical intersections (CIs) which could account for the faster decay of photoexcited *m*-MA. Indeed, as

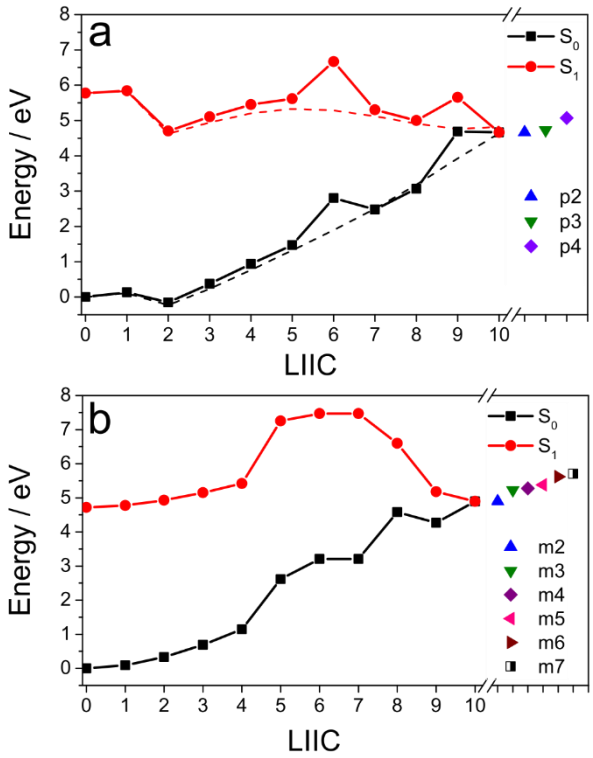

Figure 4: a) Potential energy cut along the LIIC between the *p*-MA Franck-Condon region (step 0) to **p1** (step 10). The dashed lines are along a similar coordinate without an amine rotation (see text and SM for details). b) Potential energy cut along the LIIC between the *m*-MA Franck-Condon region (step 0) to **m1** (step 10). Energies for the other CIs are shown to the right of the breaks; structures are shown in section F of the SM.

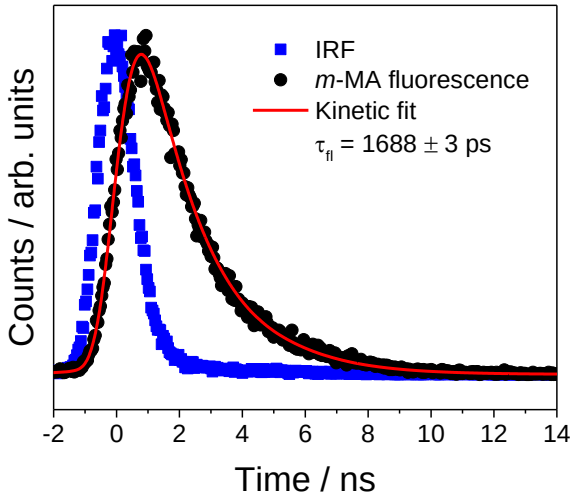

Figure 3: Fluorescence lifetime measurement for *m*-MA. Data are shown as black circles, with the red line being a kinetic fit from which a fluorescence lifetime of $\tau_{fl} \approx 1.7$ ns is obtained. The instrument response for these measurements is also shown in blue. For visual clarity, a reduced number of data points have been plotted.

shown in Figure 4, we have identified several CIs in both *p*-MA (**p1**-**p4**) and *m*-MA (**m1**-**m7**), all of which are of prefulvenic character; energies and structures for these CIs are given in section F of the SM. While any of these CIs may be accessible from the Franck-Condon region of the S_1 state, we have only sought further detail into the lowest energy CI. For both *p*-MA and *m*-MA, we have produced a PEC by evaluating the S_1 and S_0 energies along the linear interpolation of internal coordinates (LIIC) from the S_1 Franck-Condon geometry to the lowest energy CI, also shown in Figure 4. While the results from *m*-MA appear reasonable, the *p*-MA results show two features that require further comment. First, we note that the drop in *p*-MA energy away from the Franck-Condon region is an artefact of a valence state reordering and the small active space. Second, the sharp rises at steps 6 and 9 are due to the LIIC involving an amine rotation relative to the plane of the ring. Freezing the NH_2 dihedral angles at their S_0 equilibrium values results in the smoother, dashed lines also shown in Fig. 4a (see section F of the SM for further discussion of this alternate coordinate).

For both molecules, the LIIC results presented in Figure 4 suggest excited state barriers

between the Franck-Condon region and the lowest energy CIs, with the important caveat that an LIIC will be an upper bound to the true minimum energy path. While the calculated *p*-MA barrier appears to support the conclusion that *p*-MA photoexcited at the S_1 origin is trapped and is unable to access a CI, the drop in energy along the *p*-MA LIIC (as discussed above) hinders a more detailed assessment. Nevertheless, our previous conclusions remain the most likely: the trapped excited *p*-MA population must relax *via* slow ISC or weak fluorescence, in agreement with previous frequency-resolved measurements.[17,20,27]

Regardless of the substantial excited state barrier in Figure 4b, photoexcitation of *m*-MA above the S_1 origin does accelerate its excited state decay from 2.3 ns (at λ_{pu} = 325 nm) to 1.4 ns (at λ_{pu} = 300 nm). Though we again note that ISC and fluorescence likely play a role in the excited state decay of *m*-MA, the decrease in lifetime upon photoexcitation with higher energies are consistent with additional decay pathways (*e.g.* additional CIs) becoming accessible with increasing photoexcitation energy (see references 12 and 52 for example); indeed, the large number of low-lying, prefulvenic *m*-MA CIs reinforces this conclusion. Furthermore, as illustrated in Figure 5, several of the CIs found appear to be quite similar, related by mirror planes (**m1** and **m2**), functional group rotations (**m1** and **m6**), or further motion along a prefulvenic coordinate (**m1** and **m7**). From these results, and computational work on the related molecule aniline,[53] we speculate that there are many seams of intersection between the S_1 and S_0 states. We therefore conclude that while some of the excited state decay of *m*-MA must be radiative, as previously reported,[20,21,43] the relatively rapid decay at λ_{pu} = 325 nm suggests that at least one prefulvenic S_1/S_0 CI in *m*-MA is accessible at the S_1 origin with additional CIs becoming accessible at shorter pump wavelengths.

While we are unable to firmly assign the relaxation pathway in *m*-MA, it seems clear that this molecule does not follow any of the relaxation processes commonly observed for other sunscreen molecules, such as *cis/trans* isomerisation or excited state H-atom transfer,[11] instead potentially accessing prefulvenic CIs. We therefore suggest that further exploration of prefulvenic relaxation pathways may inform future sunscreen development, for which this alternative energy dissipation mechanism is optimised.

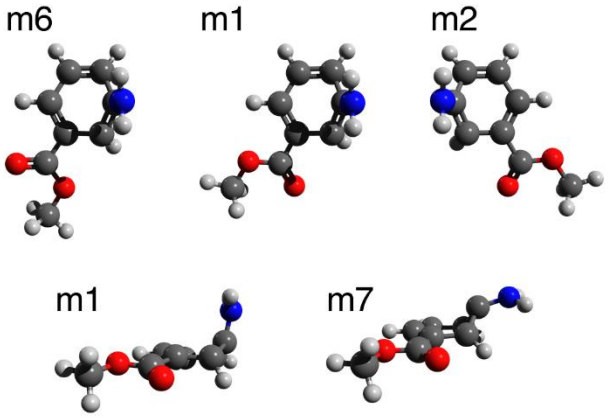

Figure 5: Example S_1/S_0 conical intersection from *m*-MA; CIs are labelled as in the text and SM. The top row highlight structures related by mirror planes or ester rotations. The bottom row shows two structures at different points along the prefulvenic coordinate.

Conclusion

Our previous study of the sunscreen precursor *o*-MA, for which an intramolecular hydrogen bond stabilises the S_1 state, revealed a long, excited state lifetime; a sub-optimal result for a sunscreen molecule. In the present work, we have removed the intramolecular hydrogen bond in two structural isomers of *o*-MA. For *p*-MA, the S_1 state is still long-lived, likely due to inaccessible CIs and/or a weakly fluorescent $S_1 \rightarrow S_0$ transition. In the case of *m*-MA, a significantly faster excited state decay is observed. While radiative pathways still play an important role in the excited state decay of *m*-MA, we speculate that a multitude of prefulvenic CIs may be sampled following photoexcitation, resulting in an accelerated decay. Initial computational results suggest an excited state barrier to these CIs, though the comparatively short lifetime of the S_1 origin suggests at least one accessible prefulvenic relaxation pathway. The discrepancies

between the *p*-MA TR-IY and fluorescence lifetime highlight the need for future theoretical and experimental work to systematically build molecular and environmental complexity.

The work presented herein demonstrates how a systematic study of the effects of molecular structure, in this case substituent position, may inform the targeted molecular design of new sunscreen molecules. Namely, we sought to explore the photophysical impact of disturbing the intramolecular hydrogen bond present in the previously studied *o*-MA. With these studies, not only have we established that the excited state decay is more efficient in *m*-MA than in the sunscreen precursor *o*-MA, but we also suggest that this enhanced decay may be due to the existence of prefulvenic S_1/S_0 CIs, which are not typically considered for other common sunscreen molecules.[11] Thus, we have unveiled an alternative relaxation pathway, the use of which may be further exploited in the context of developing a rationale for sunscreen design targeted at optimum photoprotection. We close by noting that these gas-phase studies will have to be expanded towards commercial product environments, since any sunscreen molecule candidate will eventually be employed in complex commercial formulations. Following a *bottom-up* approach, the first step towards more realistic environments would be to evaluate the impact of solvent interactions on the observed photodynamics; these studies are currently underway in our laboratory.

Acknowledgements

The authors would like to thank the Warwick Centre for Ultrafast Spectroscopy (WCUS; go.warwick.ac.uk/wcus) for use of the Cary 60 UV/Vis spectrophotometer and Horiba Scientific Fluorolog 3. Computing facilities were provided by the Scientific Computing Research Technology Platform of the University of Warwick. N.D.N.R. and K.M.K. thank the EPSRC for doctoral funding. M.A.P.T. thanks EPSRC for a doctoral studentship through the EPSRC Centre for Doctoral Training in Molecular Analytical Science, grant number EP/L015307/1. N.C.C.F. and G.W.R. thank the Leverhulme Trust for postdoctoral funding. N.D.M.H. acknowledges support from the EPSRC (Grant No. EP/P02209X/1). V.G.S. thanks the EPSRC for equipment grants (EP/J007153 and EP/N010825) and the Royal Society and Leverhulme Trust for a Royal Society Leverhulme Trust Senior Research Fellowship.

Data Accessibility

All data underpinning the present work are presented herein. Example computational input and output files, as well as all CI geometries, are available at the Zenodo Archive at doi: 10.5281/zenodo.1255999.

Declaration of interest: none.

References

(1) Takahashi, S.; Badger, M. R. Photoprotection in Plants: A New Light on Photosystem II Damage. *Trends Plant Sci* **2011**, *16* (1), 53–60.

(2) D'Orazio, J.; Jarrett, S.; Amaro-Ortiz, A.; Scott, T. UV Radiation and the Skin. *Int. J. Mol. Sci.* **2013**, *14* (6), 12222–12248.

(3) Sinha, R. P.; Häder, D.-P. UV-Induced DNA Damage and Repair: A Review. *Photochem. Photobiol. Sci.* **2002**, *1* (4), 225–236.

(4) Xue, L.; Zhang, Y.; Zhang, T.; An, L.; Wang, X. Effects of Enhanced Ultraviolet-B Radiation on Algae and Cyanobacteria. *Crit. Rev. Microbiol.* **2005**, *31* (2), 79–89.

(5) Diffey, B. L. Solar Ultraviolet Radiation Effects on Biological Systems. *Phys. Med. Biol.* **1991**, *36* (3), 299–328.

(6) Sklar, L. R.; Almutawa, F.; Lim, H. W.; Hamzavi, I. Effects of Ultraviolet Radiation, Visible Light, and Infrared

Radiation on Erythema and Pigmentation: A Review. *Photochem. Photobiol. Sci.* **2013**, *12* (1), 54–64.

(7) Brenner, M.; Hearing, V. J. The Protective Role of Melanin Against UV Damage in Human Skin†. *Photochem. Photobiol.* **2008**, *84* (3), 539–549.

(8) *Principles and Practice of Photoprotection*; Wang, S. Q., Lim, H. W., Eds.; Springer International Publishing: Cham, 2016.

(9) Baker, L. A.; Stavros, V. G. Observing and Understanding the Ultrafast Photochemistry in Small Molecules: Applications to Sunscreens. *Sci. Prog.* **2016**, *99* (3), 282–311.

(10) Rodrigues, N. D. N.; Staniforth, M.; Stavros, V. G. Photophysics of Sunscreen Molecules in the Gas Phase: A Stepwise Approach towards Understanding and Developing next-Generation Sunscreens. *Proc. R. Soc. A Math. Phys. Eng. Sci.* **2016**, *472* (2195), 20160677.

(11) Rodrigues, N. D. N.; Stavros, V. G. From Fundamental Science to Product: A Bottom-up Approach to Sunscreen Development. *Sci. Prog.* **2018**, *101* (1), 8–31.

(12) Rodrigues, N. D. N.; Cole-Filipiak, N. C.; Horbury, M. D.; Staniforth, M.; Karsili, T. N. V.; Peperstraete, Y.; Stavros, V. G. Photophysics of the Sunscreen Ingredient Menthyl Anthranilate and Its Precursor Methyl Anthranilate: A Bottom-up Approach to Photoprotection. *J. Photochem. Photobiol. A Chem.* **2018**, *353*, 376–384.

(13) Grabowski, Z. R.; Rotkiewicz, K.; Rettig, W. Structural Changes Accompanying Intramolecular Electron Transfer: Focus on Twisted Intramolecular Charge-Transfer States and Structures. *Chem. Rev.* **2003**, *103* (10), 3899–4032.

(14) Wong, T.; Orton, D. Sunscreen Allergy and Its Investigation. *Clin. Dermatol.* **2011**, *29* (3), 306–310.

(15) Weersink, R. A.; Wallace, S. C. Complexes of Methyl 4-(N,N-Dimethylamino)Benzoate: Spectroscopy and Dynamics of the Charge Transfer State. *J. Phys. Chem.* **1994**, *98* (42), 10710–10719.

(16) Howell, R.; Phillips, D.; Petek, H.; Yoshihara, K. Fluorescence of Jet-Cooled Dimethylamino Benzonitrile, Its Aggregates and Solvated Complexes. *Chem. Phys.* **1994**, *188* (2–3), 303–316.

(17) Longarte, A.; Fernández, J. A.; Unamuno, I.; Castaño, F. Ground and First Electronic Excited State Vibrational Modes of the Methyl-p-Aminobenzoate Molecule. *Chem. Phys. Lett.* **1999**, *308* (5–6), 516–522.

(18) Chakraborty, A.; Kar, S.; Nath, D. N.; Guchhait, N. Photoinduced Intramolecular Charge-Transfer Reactions in 4-Amino-3-Methyl Benzoic Acid Methyl Ester: A Fluorescence Study in Condensed-Phase and Jet-Cooled Molecular Beams. *J. Chem. Sci.* **2007**, *119* (2), 195–204.

(19) Howell, R.; Jones, A. C.; Taylor, A. G.; Phillips, D. Laser-Induced Fluorescence of Dimethylaminobenzoic Esters in Solution and Supersonic Jet. *Chem. Phys. Lett.* **1989**, *163* (4–5), 282–290.

(20) McCombie, J.; Hepworth, P. A.; Palmer, T. F.; Simons, J. P.; Walker, M. J. Conformational Analysis via LIF Spectroscopy of Jet-Cooled Molecules: Hydroxy- and Amino-Benzoic Acid Esters. *Chem. Phys. Lett.* **1993**, *206* (1–4), 37–44.

(21) Hepworth, P. A.; McCombie, J.; Simons, J. P.; Pfanstiel, J. F.; Ribblett, J. W.; Pratt, D. W. High Resolution Electronic Spectroscopy of Molecular Conformers. Methyl- and Ethyl-3-

Aminobenzoic Acid Esters. *Chem. Phys. Lett.* **1996**, *249* (5–6), 341–350.

(22) Dahl, K.; Biswas, R.; Maroncelli, M. The Photophysics and Dynamics of Diphenylbutadiene in Alkane and Perfluoroalkane Solvents. *J. Phys. Chem. B* **2003**, *107* (31), 7838–7853.

(23) Iqbal, A.; Cheung, M. S. Y.; Nix, M. G. D.; Stavros, V. G. Exploring the Time-Scales of H-Atom Detachment from Photoexcited Phenol- h 6 and Phenol- d 5 : Statistical vs Nonstatistical Decay. *J. Phys. Chem. A* **2009**, *113* (29), 8157–8163.

(24) Wells, K. L.; Perriam, G.; Stavros, V. G. Time-Resolved Velocity Map Ion Imaging Study of NH3 Photodissociation. *J. Chem. Phys.* **2009**, *130* (7), 074308.

(25) Staniforth, M.; Young, J. D.; Cole, D. R.; Karsili, T. N. V.; Ashfold, M. N. R.; Stavros, V. G. Ultrafast Excited-State Dynamics of 2,4-Dimethylpyrrole. *J. Phys. Chem. A* **2014**, *118* (46), 10909–10918.

(26) Even, U.; Jortner, J.; Noy, D.; Lavie, N.; Cossart-Magos, C. Cooling of Large Molecules below 1 K and He Clusters Formation. *J. Chem. Phys.* **2000**, *112* (18), 8068–8071.

(27) Józefowicz, M.; Heldt, J. R.; Heldt, J. Experimental and Theoretical Studies of Electronic Transition Dipole Moments of Methyl Benzoate Derivatives. *J. Lumin.* **2012**, *132* (3), 755–764.

(28) Imanbaew, D.; Gelin, M. F.; Riehn, C. Rotational and Vibrational Dynamics in the Excited Electronic State of Deprotonated and Protonated Fluorescein Studied by Time-Resolved Photofragmentation in an Ion Trap. *Struct. Dyn.* **2016**, *3* (4), 043211.

(29) Valiev, M.; Bylaska, E. J.; Govind, N.; Kowalski, K.; Straatsma, T. P.; Van Dam, H. J. J.; Wang, D.; Nieplocha, J.; Apra, E.; Windus, T. L.; et al. NWChem: A Comprehensive and Scalable Open-Source Solution for Large Scale Molecular Simulations. *Comput. Phys. Commun.* **2010**, *181* (9), 1477–1489.

(30) Humphrey, W.; Dalke, A.; Schulten, K. VMD: Visual Molecular Dynamics. *J. Mol. Graph.* **1996**, *14* (1), 33–38.

(31) Adamo, C.; Barone, V. Toward Reliable Density Functional Methods without Adjustable Parameters: The PBE0 Model. *J. Chem. Phys.* **1999**, *110* (13), 6158–6170.

(32) Dunning, T. H. Gaussian Basis Sets for Use in Correlated Molecular Calculations. I. The Atoms Boron through Neon and Hydrogen. *J. Chem. Phys. 90* (2), 1007–1023.

(33) Werner, H.; Meyer, W. A Quadratically Convergent MCSCF Method for the Simultaneous Optimization of Several States. *J. Chem. Phys.* **1981**, *74* (10), 5794–5801.

(34) Szalay, P. G.; Müller, T.; Gidofalvi, G.; Lischka, H.; Shepard, R. Multiconfiguration Self-Consistent Field and Multireference Configuration Interaction Methods and Applications. *Chem. Rev.* **2012**, *112* (1), 108–181.

(35) Møller, C.; Plesset, M. S. Note on an Approximation Treatment for Many-Electron Systems. *Phys. Rev.* **1934**, *46* (7), 618–622.

(36) Andersson, K.; Malmqvist, P. A.; Roos, B. O.; Sadlej, A. J.; Wolinski, K. Second-Order Perturbation Theory with a CASSCF Reference Function. *J. Phys. Chem.* **1990**, *94* (14), 5483–5488.

(37) Andersson, K.; Malmqvist, P.; Roos, B. O. Second- order Perturbation Theory with a Complete Active Space Self-consistent Field Reference Function. *J. Chem. Phys.* **1992**, *96* (2), 1218–1226.

(38) Hehre, W. J.; Stewart, R. F.; Pople, J.

A. Self- Consistent Molecular- Orbital Methods. I. Use of Gaussian Expansions of Slater- Type Atomic Orbitals. *J. Chem. Phys.* **1969**, *51* (6), 2657–2664.

(39) Ditchfield, R.; Hehre, W. J.; Pople, J. A. Self- Consistent Molecular- Orbital Methods. IX. An Extended Gaussian-Type Basis for Molecular- Orbital Studies of Organic Molecules. *J. Chem. Phys.* **1971**, *54* (2), 724–728.

(40) M. J. Frisch, G. W. Trucks, H. B. Schlegel, G. E. Scuseria, M. A. Robb, J. R. Cheeseman, J. A. Montgomery, Jr., T. Vreven, K. N. Kudin, J. C. Burant, J. M. Millam, S. S. Iyengar, J. Tomasi, V. Barone, B. Mennucci, M. Cossi, G. Scalmani, N. Rega, G. A. Pet, and J. A. P. Gaussian 03, Revision C.02. Gaussian, Inc.: Wallingford CT 2004.

(41) Aleksiejew, M.; Heldt, J. R. Experimental and Theoretical Studies of Electronic Energy States of Methyl Benzoate Derivatives. *J. Lumin.* **2007**, *126* (2), 665–676.

(42) El-Sayed, M. A. Triplet State. Its Radiative and Nonradiative Properties. *Acc. Chem. Res.* **1968**, *1* (1), 8–16.

(43) Carsey, T. P.; Findley, G. L.; McGlynn, S. P. Systematics in the Electronic Spectra of Polar Molecules. 1. Para-Disubstituted Benzenes. *J. Am. Chem. Soc.* **1979**, *101* (16), 4502–4510.

(44) Sobolewski, A. L.; Domcke, W.; Dedonder-Lardeux, C.; Jouvet, C. Excited-State Hydrogen Detachment and Hydrogen Transfer Driven by Repulsive 1πσ* States: A New Paradigm for Nonradiative Decay in Aromatic Biomolecules. *Phys. Chem. Chem. Phys.* **2002**, *4* (7), 1093–1100.

(45) Roberts, G. M.; Stavros, V. G. The Role of Πσ* States in the Photochemistry of Heteroaromatic Biomolecules and Their Subunits: Insights from Gas-Phase Femtosecond Spectroscopy. *Chem. Sci.* **2014**, *5* (5), 1698.

(46) Greenough, S. E.; Horbury, M. D.; Thompson, J. O. F.; Roberts, G. M.; Karsili, T. N. V.; Marchetti, B.; Townsend, D.; Stavros, V. G. Solvent Induced Conformer Specific Photochemistry of Guaiacol. *Phys. Chem. Chem. Phys.* **2014**, *16* (30), 16187.

(47) Horbury, M. D.; Baker, L. A.; Quan, W.-D.; Young, J. D.; Staniforth, M.; Greenough, S. E.; Stavros, V. G. Bridging the Gap between the Gas Phase and Solution Phase: Solvent Specific Photochemistry in 4- Tert - Butylcatechol. *J. Phys. Chem. A* **2015**, *119* (50), 11989–11996.

(48) Melhuish, W. H. QUANTUM EFFICIENCIES OF FLUORESCENCE OF ORGANIC SUBSTANCES: EFFECT OF SOLVENT AND CONCENTRATION OF THE FLUORESCENT SOLUTE 1. *J. Phys. Chem.* **1961**, *65* (2), 229–235.

(49) Taylor, P. R. On the Origins of the Blue Shift of the Carbonyl N-.Pi.* Transition in Hydrogen-Bonding Solvents. *J. Am. Chem. Soc.* **1982**, *104* (19), 5248–5249.

(50) Karelson, M.; Zerner, M. C. On the N-.Pi.* Blue Shift Accompanying Solvation. *J. Am. Chem. Soc.* **1990**, *112* (25), 9405–9406.

(51) Hochstrasser, R. M. Analytical and Structural Aspects of Vibronic Interactions in the Ultraviolet Spectra of Organic Molecules. *Acc. Chem. Res.* **1968**, *1* (9), 266–274.

(52) Young, J. D.; Staniforth, M.; Chatterley, A. S.; Paterson, M. J.; Roberts, G. M.; Stavros, V. G. Relaxation Dynamics of Photoexcited Resorcinol: Internal Conversion versus H Atom Tunnelling. *Phys. Chem. Chem. Phys.* **2014**, *16* (2), 550–562.

(53) Sala, M.; Kirkby, O. M.; Guérin, S.; Fielding, H. H. New Insight into the Potential Energy Landscape and Relaxation Pathways of Photoexcited Aniline from CASSCF and XMCQDPT2 Electronic Structure Calculations. *Phys. Chem. Chem. Phys.* **2014**, *16* (7), 3122–3133.